Journal of Hydrology: Regional Studies 43 (2022) 101206

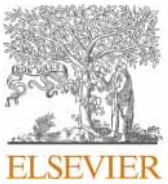

Contents lists available at ScienceDirect

Journal of Hydrology: Regional Studies

journal homepage: www.elsevier.com/locate/ejrh

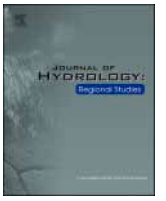

Effect of fast drainage in karst sinkholes on surface runoff in Larzac Plateau, France

P. Fischer *, S. Pistre, P. Marchand

HydroSciences Montpellier, Univ. Montpellier, CNRS, IRD, Montpellier, France

ARTICLE INFO

Keywords:
Karst
Interface
Flood
Hydrology
Modeling
Mediterranean

ABSTRACT

Study region: A 1 km^2 mountainous karst watershed on the Larzac Plateau in Southern France.
Study focus: The village of La Vacquerie, located at the outlet of the watershed, is punctually affected by flash floods during storm events. On the contrary, no runoff is observed in the village during other rainfalls. A sinkhole, draining surface flows at the entrance of the village, plays a role on these differences. Descriptions of short and intense rainfalls in 2015 (avg. 40 mm/h over 5 h) and long and light events in 2014/2016 (avg. 8 mm/h over 25 h) provide valuable data to calibrate inputs of a distributed physic-based flow model, in particular the sinkhole drainage capacity. This study aims to quantify drainage capacity changes with rainfall characteristics and to find the rain intensity threshold at which runoff exceeds sinkhole capacity.
New hydrological insights for the region: The hydrological water balance of the hydrosystem is affected by the intensity variations for each of the different rain events. It shows the limited part of drainage in sinkhole (10%) during long light rains but its significant increase (40%) during short and intense rains. Drainage in sinkhole is affected by intensity variations rather than by the total amount of precipitation. When intensity exceeds 110 mm/h the sinkhole is submerged. However, this result is obtained in a case of Plateau configuration, where the saturated level, located deep below the surface (here 500 m), does not retro-affect drainage in the sinkhole.

1. Introduction

Hydrological investigations aim at quantifying the repartition of rain water among surface flow (through runoff) and the different underground reservoirs (through infiltration) of a watershed. The determination of these exchanges between surface and subsurface become even more crucial when considering extreme events (floods or droughts). In karstic environments, the underground domain is highly contrasted between low-permeability limestone rocks and the network of conductive fractures or conduits enlarged by dissolution through groundwater flows. This specificity in karst environments is source of additional challenges for hydrological and hydrogeological sciences (White, 2002; Ford and Williams, 2007). Therefore, hydrological case studies on karst are often site-specific as the existing contrasts in such medium, and thus its complex hydrological responses, are closely related to a karstogenesis that is related to the geological and climatologic history of a region. These contrasts can also be found at the surface, in the epikarst, where surface-subsurface exchanges are slow and diffuse in soils while they can be fast in the fracture networks and almost instantaneous but localized in sinkholes or losses (Klimchouk, 1995).

The hydrological processes controlling the infiltration rates and the generation of runoff have been studied on a mountainous karst

* Corresponding author.
E-mail address: pierre.fischer@umontpellier.fr (P. Fischer).

https://doi.org/10.1016/j.ejrh.2022.101206
Received 12 April 2022; Received in revised form 5 September 2022; Accepted 5 September 2022
Available online 8 September 2022

area in Spain in Li et al. (2011). They performed rainfall simulations on in-situ micro-plots among a karst landscape and show the role of vegetation and rock fragments on infiltrations. They quantified the averaged runoff coefficient over one year at the hillslope scale and found runoff to be globally limited (1.44%). A similar study was performed in a sub-tropical soil-epikarst system in China in Wang et al. (2020). They quantified surface, soil seepage and epikarst seepage runoffs in 20 m long in-situ hillslope plots in a 5 m width and 4 m deep trench and for artificial rainfall events at different intensities. They observed that soil seepage runoff always generated first during rain events and that surface runoff was the resultant of both a rain intensity exceeding of the soil-epikarst interface infiltration rate and a sufficient cumulated rain to saturate the soil layer.

The previously presented studies in karst system do not take impact of developed karst sinkholes or losses in the epikarst. Such structures are punctual and represent a very limited surface among karst landscapes. Nevertheless, they can still play an important role

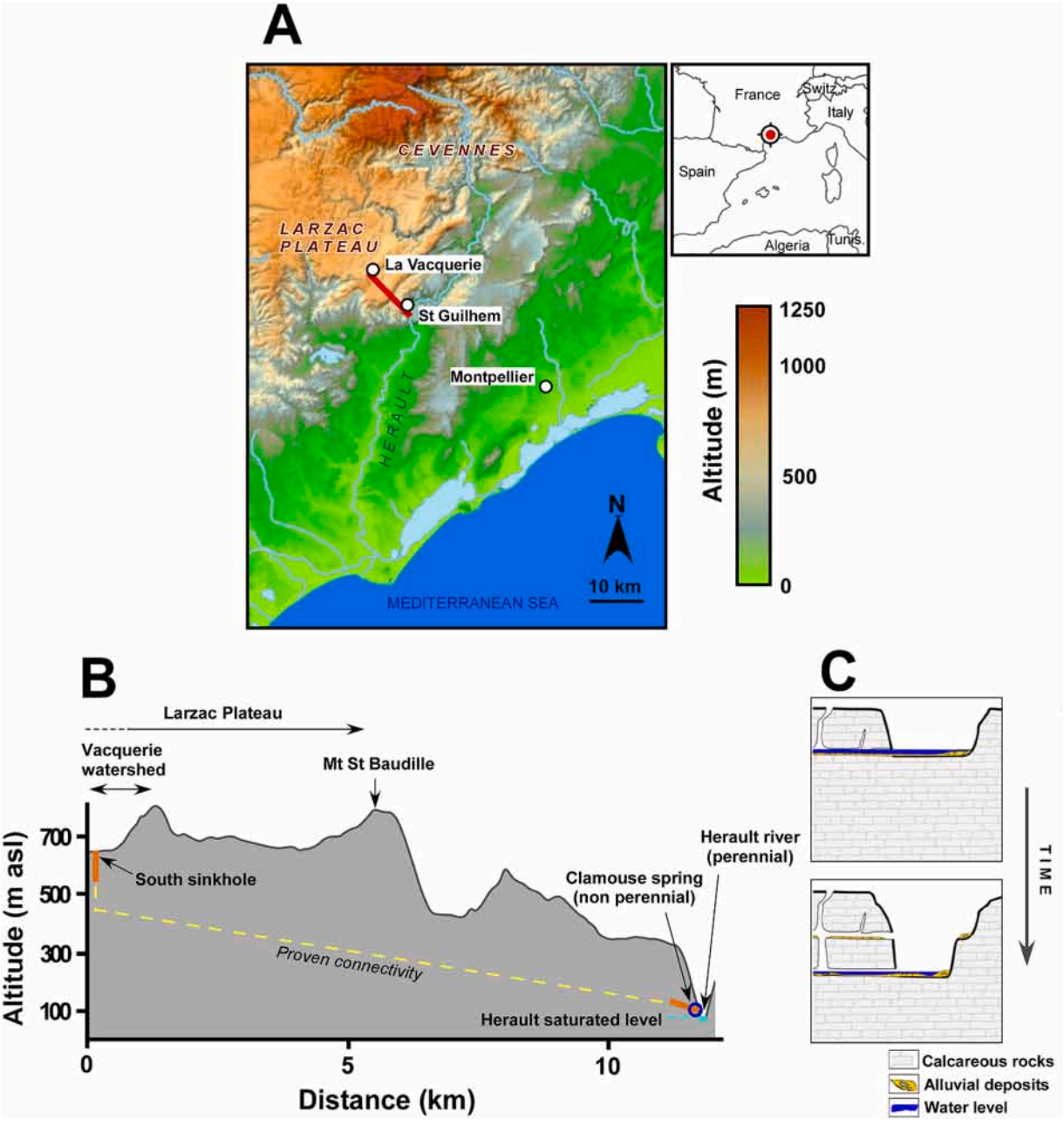

Fig. 1. A: Localization map of the study site. Elevation background map was obtained from geoportail.fr. B: Cross-section along the red line on localization map showing the underground karst connectivity between the Vacquerie sinkholes and the Hérault river canyon. C: Scheme of the constitution of an unsaturated layered karst network throughout the lowering of the Hérault river level.
Modified after Malcles et al. (2020)

on the global hydrological balance in a karst watershed, especially in relation with runoffs during intense rain events (Gutiérrez et al., 2014). According to Zhou (2007), sinkholes play a significant role in flood risks on karst terranes. In particular, a 'recharge-related flooding' is defined to describe floods occurring in karst landscapes when the sinkholes drainage capacities become lower than the storm water runoffs. The determination of this drainage capacity is however complex because it mainly depends on the sinkhole size, morphology and the configuration of the underlying karst network. Thus, Zhou (2007) advises to collect detailed information about the sinkholes in karst floods studies. Hydraulic models for quantifying drainage in sinkholes have been proposed in Field (2010), on the basis of Torricelli's theorem. However, these models require a good knowledge on sinkholes dimensions and shapes.

The role of sinkholes in local flash flood case studies has been taken into account in conceptual models. In Maréchal et al. (2008) and Fleury et al. (2013) they analyzed the spatial responses of a karst hydrosytem in Southern France to a storm event on the basis of runoff measurements at the surface, water table measured in sinkholes and the karst spring discharge. In particular they show how sinkholes near to the spring can play a role of drainage at the beginning of the event and swap to a role of 'back-flooding' when the karst network becomes totally saturated and generates backflows. In Bailly-Comte et al. (2009), similar data have been collected for another storm event in Southern France in addition to water temperature measurements in karst sinkhole. These additional temperature data allowed better identifying when sinkholes were playing a role of drainage or when they were supplying surface runoffs. If these conceptual models help understanding the global behaviors of sinkholes in terms of exchanges during rainfall event on karst terranes, they do not allow to quantify these exchanges and the drainage capacities of the sinkholes. Thus, Bailly-Comte et al. (2012) later performed a semi-distributed modeling analysis with HEC-HMS on the same hydrosystem in Southern France and could estimate the sinkholes global drainage capacities to be 7 m^3/s. Palanisamy and Workman (2015) also proposed an adaptation of the semi-distributed physical-based hydrological model SWAT in order to take the role of individual sinkholes into account. They have tested their model on a karst watershed in Kentucky and have shown that the integration of the location and mean diameter of each sinkhole significantly improved the models prediction abilities. A distributed physical-based modeling of surface runoffs and infiltration among a karst watershed has been tested in Liu et al. (2005) on a 273 km^2 catchment in Vietnam. However, at this important scale, they could not specifically quantify the role of the different sinkholes along the river. Recently a distributed combined discrete-continuum model has been proposed in Al Aamery et al. (2021) that take into account vertical exchanges between surface

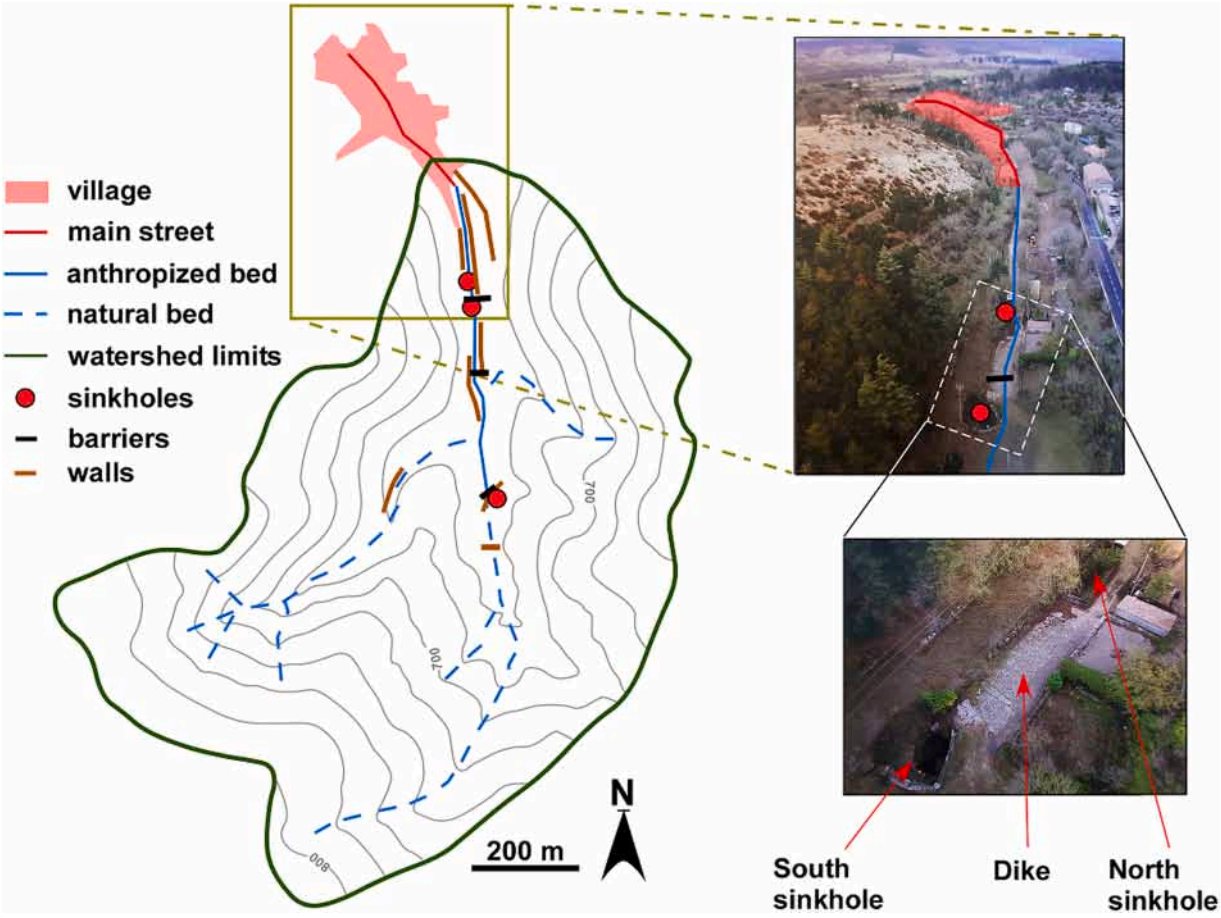

Fig. 2. Map of the watershed showing its topography, the village at the outlet, the anthropic structures and the hydrologic features. Photography credits: D. Allasia

flows and groundwater flows in a karst medium. In particular it also allows integrating punctual drainage in sinkholes. This model has been tested on a 58 km^2 karst basin in Kentucky. The requirement of an advanced knowledge on the karst underground structures for the application of such model is highlighted.

This work presents a 2D spatially distributed modeling application to simulate the hydrological responses of a small karst watershed (1 km^2) located in Southern France to four different rainfall events. These four events generate 150 to 250 mm of cumulated rain over periods ranging from 5 h to 25 h. A village is located at the outlet of the watershed. During short but intense events, important flash floods affect the village. On the contrary, during longer but lighter events, runoff is almost absent in the village. A karst sinkhole, located at the entrance of the village plays a key role on this response contrast. Due to its small size and its configuration, this watershed can be easily conceptualized and spatial modeling can contribute to the understanding of its hydrological behavior. The different karst sinkholes and losses among the watershed have been individually identified and characterized so that performing a quantification of drainage capacity becomes possible. Furthermore, a storm event in August 2015 has been particularly described and

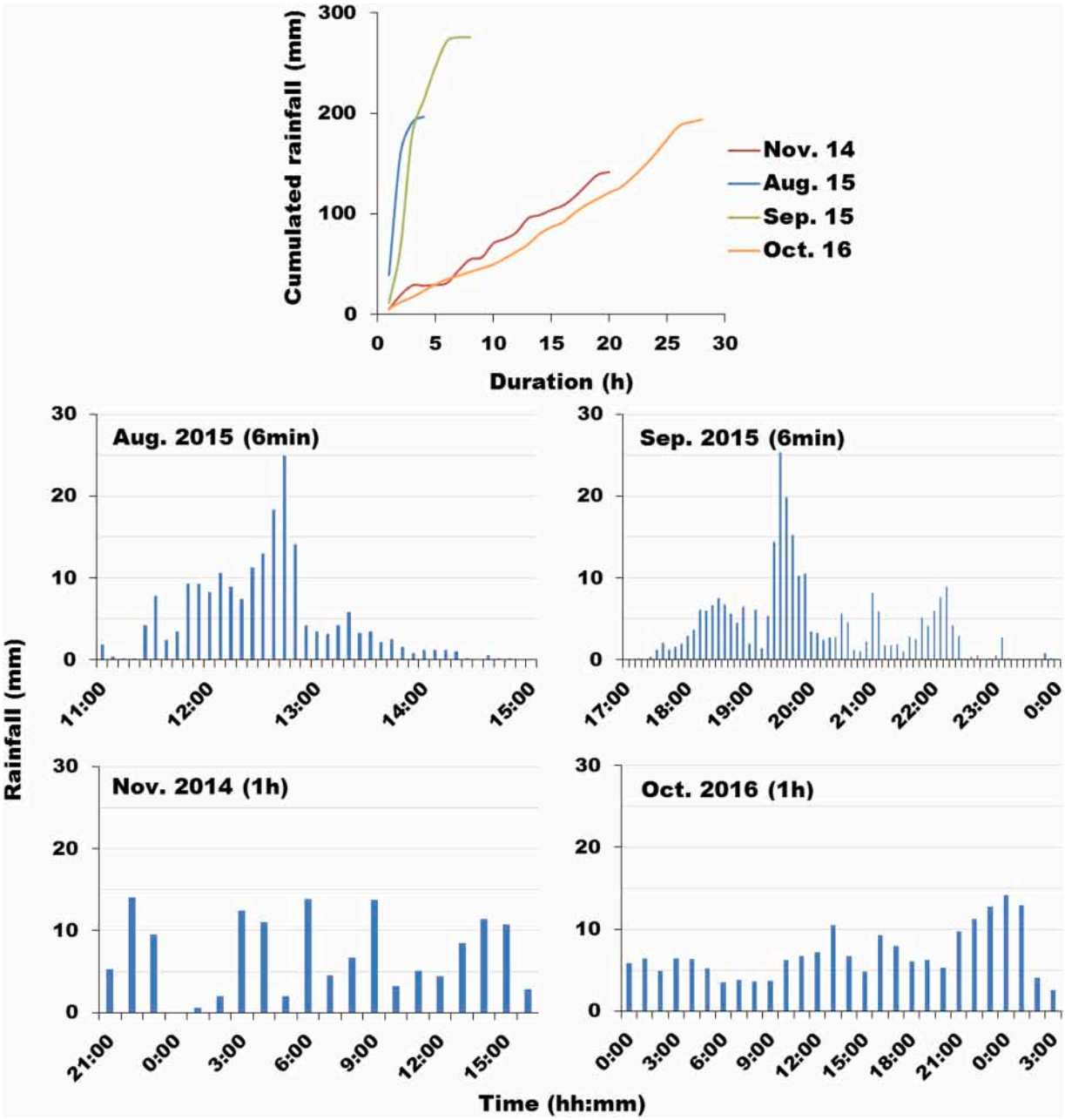

Fig. 3. Cumulated rainfall over time for four different rainfall events and their associated hyetograms. For the intense events (Aug. and Sep. 2015) the hyetogram time step is 6 min, while for the long events (Nov. 2014 and Oct. 2016) it is 1 h.

provides valuable data to calibrate the model. Thus, this study site represents a particularly interesting case in order to more generally investigate the effect of water runoffs drainage in karst network through surface sinkholes on global runoff at the outlet of the hydrosystem.

2. Presentation of the study site

2.1. Hydrogeological context

The study case presented in this work is based on a small 1 km^2 watershed located at the periphery of the Larzac Plateau, between the Cevennes Mountain and the Mediterranean sea in the South of France (Fig. 1a). At the outlet of this watershed is located the village of La-Vacquerie-et-Saint-Martin-de-Castries, hereafter reduced to 'La Vacquerie' (Fig. 2). The watershed is localized at quite high altitudes, between 630 and 800 m asl. It is typical for mountainous watersheds, characterized by important slopes.

The underground of the watershed is composed of fractured Bajocian dolomites and Oxfordian limestones. These carbonated formations are karstified. Three important karst structures (North sinkhole, South sinkhole and Vacquerie Loss) can be found at the surface. In particular the South sinkhole forms a large depression at the surface extending among a diameter of 8 m and a depth of 6 m. A speleological investigation has shown that it vertically extends to, at least, a depth of 109 m where a constriction prevents deeper progress (see Fig. S2). Tracer tests have shown that the South sinkhole is connected to the Clamouse karst system located in the Hérault river canyon, near Saint-Guilhem-le-Désert (Fig. 1b). The Clamouse spring is a non-perennial spring at the outlet a multi-layered sub-horizontal unsaturated karst system visited along 500 m. Camus (1997) and Malcles et al. (2020) have described the karstogenesis of the karst network around the Larzac Plateau: due to the digging of canyons by rivers over time, unsaturated karst levels have progressively formed in multi-layered systems (Fig. 1c). As the current saturated level in at the altitude of the Hérault river (100 m asl), nowadays the studied watershed lies over a 500 m deep layered unsaturated karst conduits network.

The watershed is mostly covered by scrublands on the fractured calcareous rocks outcrops with only a few centimeters of soils. In some areas, the soils become thicker and allow the development of denser vegetation (conifers, hardwoods, grass). However, globally, the soil thickness barely exceeds one meter over the calcareous rocks among the area. These soils partially cover the well-developed karst system. The average vertical permeability of the karst is assumed to be higher than that of the soils and therefore sufficient to evacuate the infiltrated water to deep levels.

2.2. Catastrophic flood events

This Mediterranean area is subject to extreme storm event due to the Cevennes reliefs that block and concentrate the humid air coming from the sea. One particularity of the village of La Vacquerie is that its main street corresponds to the outlet of the watershed (Fig. 2). Thus, in this context of Mediterranean intense storm event, the village is often subject to fast and torrential floods. Nevertheless, through time, villagers have tried to take advantages of the environment of the watershed to counterbalance this hydrological risk. In particular, they have understood the role of drainage played by the karst sinkholes and losses during the flood events and have built barriers and walls to lead water to them. An historical study of these adaptions is described in Leblanc (2018) and summarized in Fig. S1 of the supplementary files. A geomorphological description of the different sinkholes among the watershed and the anthropic structures built around them is proposed in Fig. S2 of the supplementary files.

Currently, when runoff appears during a storm event, water flows preferentially along natural and anthropized streambeds (which are usually dry) until it reaches a dike located at the entrance of the village and built in front of the South sinkhole in order to both protect the village and favor drainage in the sinkhole. The two other sinkholes of the watershed have been used as flood protection by villagers in the past but are now almost entirely clogged.

Despite these natural and anthropic protections, flooding of the village still occurs during some particularly intense storm events. In particular, in 2015, two extreme events in August and September have both resulted in catastrophic fast and torrential floods in the main street of the village. According to the meteorological data presented in Bois et al. (1997), these two events have a return period of more than 100 years. Fig. 3 presents the hyetographs of these two storm events, in comparison to two other rainfall events from November 2014 and October 2016 generating similar magnitudes of cumulated rainfalls over the watershed but no flood and associated to return periods of 10 years according to Bois et al. (1997).

It is obvious that rainfall intensity and karst structures play a role in the formation of flood. However, this particular study case represents an interesting possibility to quantify this role trough numerical modeling. In fact, the small size of the watershed makes it easy to characterize. Furthermore, the main street of the village is the outlet of the watershed, this street has a constant width and houses are all built in one block along each border of the street. Thus the main street forms a rectangular channel that can be used to assess the flowrate at the outlet. Fast floods occur during very limited amount of time, which make data measurement of such events very complicated. Nevertheless, the chronology of the flood event of August 2015 in La Vacquerie has been documented both during the flood and after (see Fig. S3 in the complementary files for details). On the basis of a video image processing with the freeware Fudaa LSPIV (Le Coz et al., 2010, 2014) made on six videos taken during the flood, it has been possible to estimate the velocities of the flows in the street during this event. These velocity values, associated to the water level visual estimations, are used both to calibrate the roughness of the main street and to confront the spatial numerical model.

3. Numerical model

3.1. Global presentation of the model

The 2D top-down view hydrological numerical model of the watershed is created in the modeling software Hydrologic Engineering Center's River Analysis System (HEC-RAS).

Unsteady fluid flow is described by the Navier-Stokes equations, considering the Shallow Water assumptions: incompressible flow, uniform density, negligible vertical velocity (i.e. hydrostatic pressure can be assumed) and turbulence is approximated. The continuity equation then becomes:

$$\frac{\partial h}{\partial t} + \nabla \cdot (h\mathbf{V}) = q \tag{1}$$

where h is the water depth (m), $\mathbf{V}$ is the horizontal velocity vector (m/s), t represents time (s) and q is the sink/source term (i.e. in this case rainfall, infiltration and drainage).

The momentum equation becomes:

$$\frac{\partial \mathbf{V}}{\partial t} + (\nabla \cdot \mathbf{V})\mathbf{V} + f_c \times \mathbf{V} = -g\nabla z_{ws} + \frac{1}{h}(\boldsymbol{\nu}_t h \nabla \mathbf{V}) - \frac{\boldsymbol{\tau}_b}{\rho R} \tag{2}$$

where f_c is the Coriolis parameter unit vector, g is the gravitational acceleration (m/s^2), z_{ws} is the water table elevation, $\boldsymbol{\nu}_t$ is the eddy viscosity tensor, $\boldsymbol{\tau}_b$ is the bottom shear stress vector calculated based on the Manning coefficients, ρ is the fluid density (kg/m^3) and R is the hydraulic radius (m).

The resolution of the 2D fluid flow equations in the model is performed base on an Eulerian-Lagrangian method and a combination of finite difference and finite volume methods on a polygonal mesh. A characteristic size of 10 m for the unit mesh elements has been chosen. However, the mesh is refined in the areas surrounding the streambed (see Fig. 4b) to a size of 2 m. Furthermore, the streambed itself represents a mesh breakline where mesh is generated along the flow direction with a mesh size of 1 m. Finally, a buffer area is considered on the Larzac Plateau, downstream of the watershed, which is meshed with a characteristic cell size of 20 m. In total the mesh is composed of 22500 cells. In each mesh cell, a hydrological water budget is computed based on lateral and rainfall incomes and losses through infiltration and runoffs in order to update the local water depth. Underground flow processes in the karst conduits network are not considered explicitly in this model, all infiltrated water is considered to be lost in the simulations. However the model quantifies in each cell the water exiting the model through infiltration. Therefore we can pay particular attention to the volume and flow lost through absorption locally in the sinkholes and have an estimation of its consistency based on the sinkholes dimension. The boundary conditions of the model are no flow conditions as the boundaries follow the limits of the watershed. The large buffer area

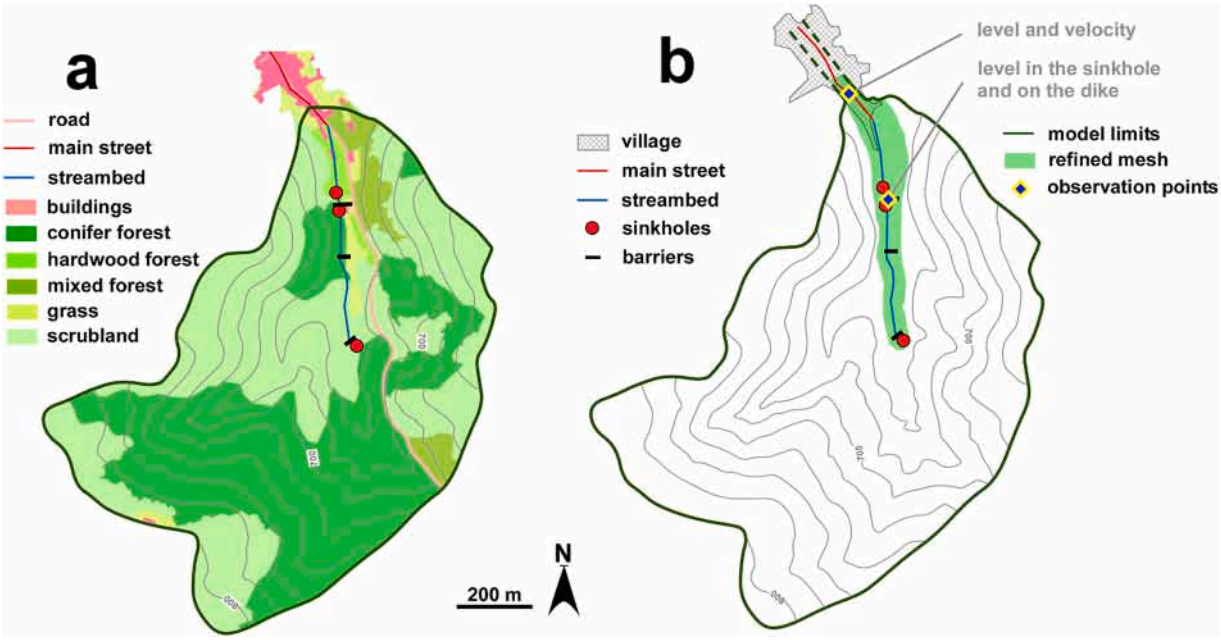

Fig. 4. a: Map of the different biomes present among the watershed that is used as a basis to implement the soil properties in the model. b: Map showing the area of mesh refinement along the main streamflow and the locations of the focus points used to compare simulation results and observations/measurements.

created downstream of the village in the model permits to limit the impact of the downstream boundary condition, as water will then reach the Larzac Plateau where it will spread without impacting the upstream flows. An unsteady flow time step of 0.5 s is chosen, based on the mean mesh size and the maximal flow velocities.

This modeling of the watershed hydrodynamics assumes different important hypotheses linked to its characteristics: i) rainfall is uniform among the watershed, ii) the watershed is at a sufficient altitude and the groundwater saturated level is sufficiently low during the intense rainfall time periods (August and September) to consider that water level in the karst network does not impact drainage in the sinkholes, iii) thus when water enters a sinkhole it is drained based on a constant flow rate value in relation to its morphology, iv) soils become quickly saturated so that diffuse infiltrations are constant and depend on the soils saturated conductivities, v) evapotranspiration and wind effects are neglected during the rain events.

In the model we considered drainage only in the South sinkhole. The other sinkholes being clogged, they contribute to diffuse infiltration in the model but not for punctual drainage. The drainage in the South sinkhole is considered to be limited by the narrowness found at 109 m depth. Thus, during storms, the sinkhole can be simplified to a funnel leading water to a filled vertical pipe draining at a constant rate conditioned by this narrowness diameter. In the model, considering the previous assumption, an equivalent drained constant rate is set in order to remove water from the model as long as there is water in the depression formed by the sinkhole in the topography. If water incomes exceed the draining rate, the depression begins to fill up.

3.2. Input and output parameters

The principal input of the model consists in the digital terrain model of the watershed with an altimetry accuracy of 1 cm and a spatial resolution of 1 m. A tacheometry campaign has been led on field in order to add to this terrain model, through GIS tools, the anthropic structures (such as building and walls) and the streambed and sinkhole surface dimensions with similar accuracies. Rainfall is then applied uniformly in the model. For the intense events (August and September 2015), the rainfalls were applied at a time step of 6 min, while for the long events (2014 and 2016), the rainfalls were applied at a time step of 1 h.

Other inputs of the model are associated to hydraulic properties of soils, such as roughness, saturated conductivities and impermeability percentage. First, the different biomes of the watershed have been spatially identified based on the French National Institute of Geographical and Forestry Information (IGN) database (Fig. 4a), which has also been verified on field and using drone aerial views.

The saturated hydraulic conductivities were assessed, for three types of soils observed among these biomes, based on the Beerkan infiltration method (Lassabatère et al., 2006). Roughness and impermeability percentage cannot be measured easily on field, thus ranges of values (a minimal, a maximal and a plausible value between them) were estimated for each biome based on tables and visual observations. The input values used for these three properties are listed in Table 1.

Simulation allows to assess water level and velocity spatially. However, in order to compare the simulation to real observations, we have especially selected two observations points in the model (see Fig. 4b). One observation point is in the main street of the village were the water depth and the velocity in the street can be compared to the visual or video information of each event. The other observation point concerns the water table elevation at the sinkhole and the dike in order to check potential overflowing of these structures.

4. Simulations results

4.1. Calibration with the 23th August 2015 event

The model has first been calibrated with the rainfall event of August 2015, before being validated on the other events. In particular the constant drainage rate of the South sinkhole has been optimized in order to mimic the numerous observations of the catastrophic

Table 1
Soil properties associated to infiltrations capacities and surface roughness in the different biomes. For the measured saturated conductivities, an uncertainty of 50% on the measure has been considered for the sensitivity analysis. For the unmeasurable properties (roughness and percent of impermeable surfaces) a value has been selected among a range that will be used to check the sensitivity of the model.

Biome	Sat. conductivity (m/s) [min; measured; max]	Manning values [min; chosen; max]	Impervious (%) [min; chosen; max]
WATERSHED			
Conifer forest	0.7; 1.4; 2.1 ($\times 10^{-4}$)	0.08; 0.15; 0.18	0; 10; 15
Hardwood forest	0.5; 1.0; 1.5 ($\times 10^{-5}$)	0.025; 0.07; 0.1	0; 5; 15
Mixed forest	1.8; 3.7; 5.6 ($\times 10^{-6}$)	0.025; 0.04; 0.1	0; 5; 15
Grass	0.5; 1.0; 1.5 ($\times 10^{-5}$)	0.025; 0.04; 0.1	0; 0; 0
Scrubland	1.8; 3.7; 5.6 ($\times 10^{-6}$)	0.025; 0.03; 0.05	0; 0; 10
STREAMBED			
Asphalt	0	0.013; 0.014; 0.015	100; 100; 100
Cement	0	0.011; 0.015; 0.02	100; 100; 100
Path	1.8; 3.7; 5.6 ($\times 10^{-6}$)	0.023; 0.03; 0.04	0; 0; 5
Rocks	0	0.023; 0.03; 0.03	100; 100; 100
Light vegetation	0.5; 1.0; 1.5 ($\times 10^{-5}$)	0.03; 0.05; 0.06	0; 20; 30
Dense veget.	0.5; 1.0; 1.5 ($\times 10^{-5}$)	0.1; 0.15; 0.2	0; 50; 100

event. Thus, 9 simulations on this event have been performed with drainage rates increasing from 0 to 40 m^3/s. Overall, simulation obtained with a sinkhole drainage of 20 m^3/s appeared to provide the most coherent behaviors at observations points (Fig. 5). In particular, in the main street, a peak water level of 49 cm with a peak velocity of 5.1 m/s are simulated. Real observation of this event mentions a peak level of approximately 50 cm and videos interpretations reveal velocities reaching at least 4 m/s. However, according to ocular observations during the event the level in the street has quickly risen at the peak and remained at a high level during one hour before starting decreasing at 1.20 pm. In the simulation the water level indeed rises in 15 min before reaching the peak but then immediately decreases and remains at 10 cm until 1.20 pm. Thus, the simulation doesn't show a one hour peak level plateau.

Post-event observations in the watershed mention that both sinkholes (North and South) and the loss were flooded and that a floodplain of 100 m length has formed between the dike and the debris barrier. All these observations are also simulated with the model (Figs. 5 and 6). Furthermore, in the simulation, the dike was overflown under at most 31 cm of water, which corresponds to the observed high-water marks.

In order to check the consistency of the drainage of 20 m^3/s in the sinkhole, we have applied the Torricelli's formula adaptation presented in Field (2010), considering the sinkhole to have a conic shape, and the Hazen and Williams (1920) formula of pipe flows, considering the sinkhole to be similar to a continuous vertical pipe of 109 m. In both cases, in order to obtain such maximal rate, we find that the diameter of the minimal section of the sinkhole structure should be between 75 and 100 cm. These values appear as rather realistic in regards to the observed shrinkage that blocked the speleologists' progression at 109 m depth.

The water levels and velocities simulated in the main street in the 9 scenarii (with increasing sinkhole drainage) and plotted in Fig. 7. It shows that the peak in the street is directly correlated to drainage of the South sinkhole. In fact, between 0 and 20 m^3/s, the higher the drainage, the lower the peak level and velocity in the street. Over 20 m^3/s, the peak level and velocity remain approximately the same. Looking at the simulations in these cases and especially the water level in the sinkhole (Fig. 7), one notes that this is related to the fact the sinkhole is no more totally submerged. An interesting simulated observation (that even remains for all drainage rates over 20 m^3/s) is that the dike remains submerged even if the sinkhole is not. This is due to the configuration of the area and the high velocity of the flows upstream from the dike: a rotational flow forms over the sinkhole which allows some of the water at the exterior of the vortex to pass over the dike. It can also be noted that without the role of the sinkhole (i.e. when drainage rate is considered to be 0 m^3/s), peak water level in the street would be 1.25 m instead of 49 cm. This shows the importance of the South sinkhole and the structures built around it to protect the village.

If the model can indeed simulate most of the observations, it can remain questionable due to some of its inputs (i.e. Manning coefficients and impermeability percentages) uncertainties. Thus, a sensibility analyses are required to test the robustness of this calibration.

4.2. Sensibility analyses

Three basic analyses were conducted on the Manning value inputs, the soils impermeability ratio inputs and on the infiltration rates. They consist in comparing the simulated water velocity in the main street during the August 2015 event, considering the sinkhole drainage rate previously calibrated for this event (i.e. 20 m^3/s). This comparison, presented in Fig. 8 and Fig. 9, is performed each time with three scenarii: simulation using the minimal values, the chosen values (used for the calibration) and the maximal values as presented in Table 1.

The possible range of values for the impervious parameter appears to have a negligible impact on the simulation. The range of Manning coefficients can only slightly impact the simulation results in the main street. The lowest values would accentuate the peaks, while the highest values would smooth the signal. Globally the simulations show a low sensibility to the input parameters that could not be measured, which is reassuring for the accuracy of the model.

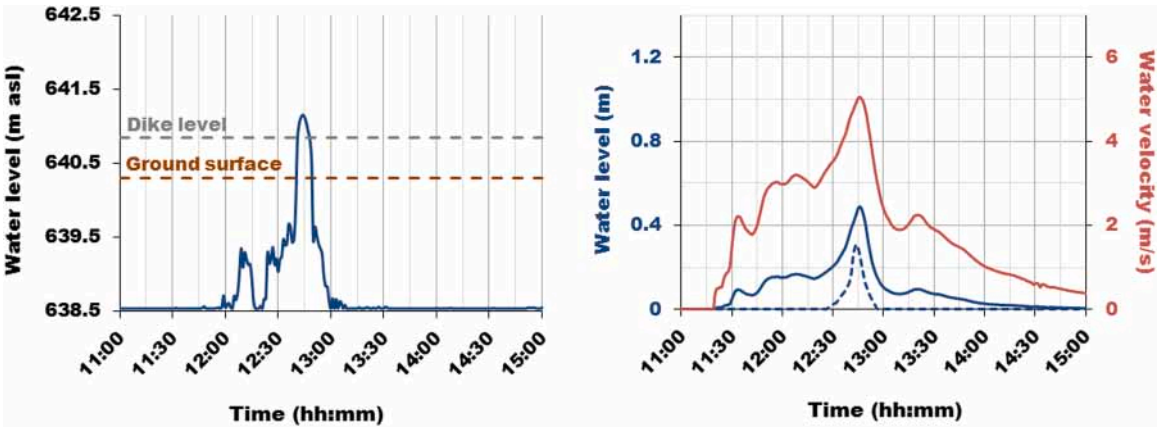

Fig. 5. Simulations results for the Aug. 2015 event considering a maximal drainage rate of 20 m^3/s. Left: Water level (in m asl) over time in the South sinkhole. The brown and grey dotted lines show the ground elevation at this location and the dike highest altitude. Right: Water level (in m) over time at the dike (dotted blue line) and in the street (full blue line) and velocity in the street (red line).

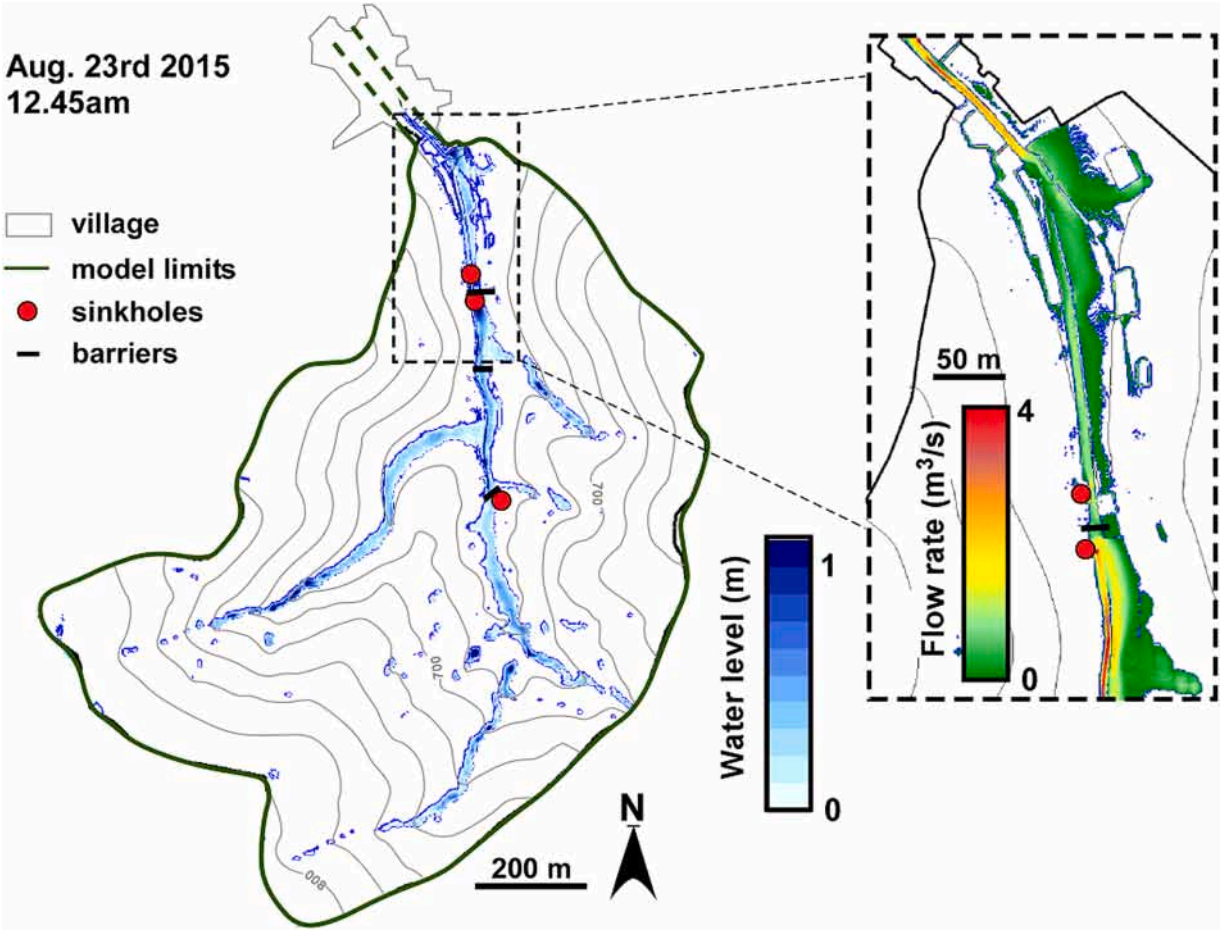

Fig. 6. Spatial simulations of water heights over the watershed at 12.45 am during the Aug. 2015 event (when the dike is overflown). The zoom box presents the simulated flow rates at the same time step between the dike and the main street in the village.

The water velocity simulated in the main street is also almost insensitive to a variation of 50% of the infiltration rates, only a slight deviation can be observed when the water level decreases. Thus, these analyses show that, in such context of torrential flows in a mountain watershed, the predominant factor influencing runoffs and flows remains indeed the morphology of the terrain. This morphological information is quite precisely integrated in the model through a high-resolution digital terrain model.

4.3. Validation on the other events

The previously calibrated sinkhole drainage rate in the model can be tested for the other rainfall events. For the three other events, we do not have as much observations as for the August 2015 event but we know that the village was not flooded during the November 2014 and October 2016 event and flooded during the September 2015 event. Thus, these model validations remain qualitative (flooded or unflooded). When performing simulations on these events with the model we reproduce a correct behavior (Fig. 10): water fluxes in the main street is negligible during the 2014 and 2016 events, while the village flooded (with an important peak due to the dike submersion) for the September 2015 event.

Furthermore, we tested other drainage rates also for these events. It can be noted that for the 2014 and 2016 events, when no drainage in the sinkhole is considered, the village becomes flooded. However a small drainage rate of 5 m^3/s was already sufficient in these cases to prevent flooding.

Concerning the September 2015 event, simulation shows a slightly less catastrophic flood than for the August 2015 event. However, according the villagers, the September event resulted in a more important flood than the one several days before. In order to explain this difference with the simulations, it shall be considered that the model considers a similar condition and sinkhole drainage for both events. In reality, after the August event, the sinkhole was partly obstructed by debris and the street downstream from the dike was destroyed. When the September event occurred, these consequences were not fixed yet and may have aggravated the flood (mainly by decreasing the drainage capacity of the sinkhole).

Table 2 summarizes the different rainfall events and their simulations results in the main street and at the dike during the peaks. It

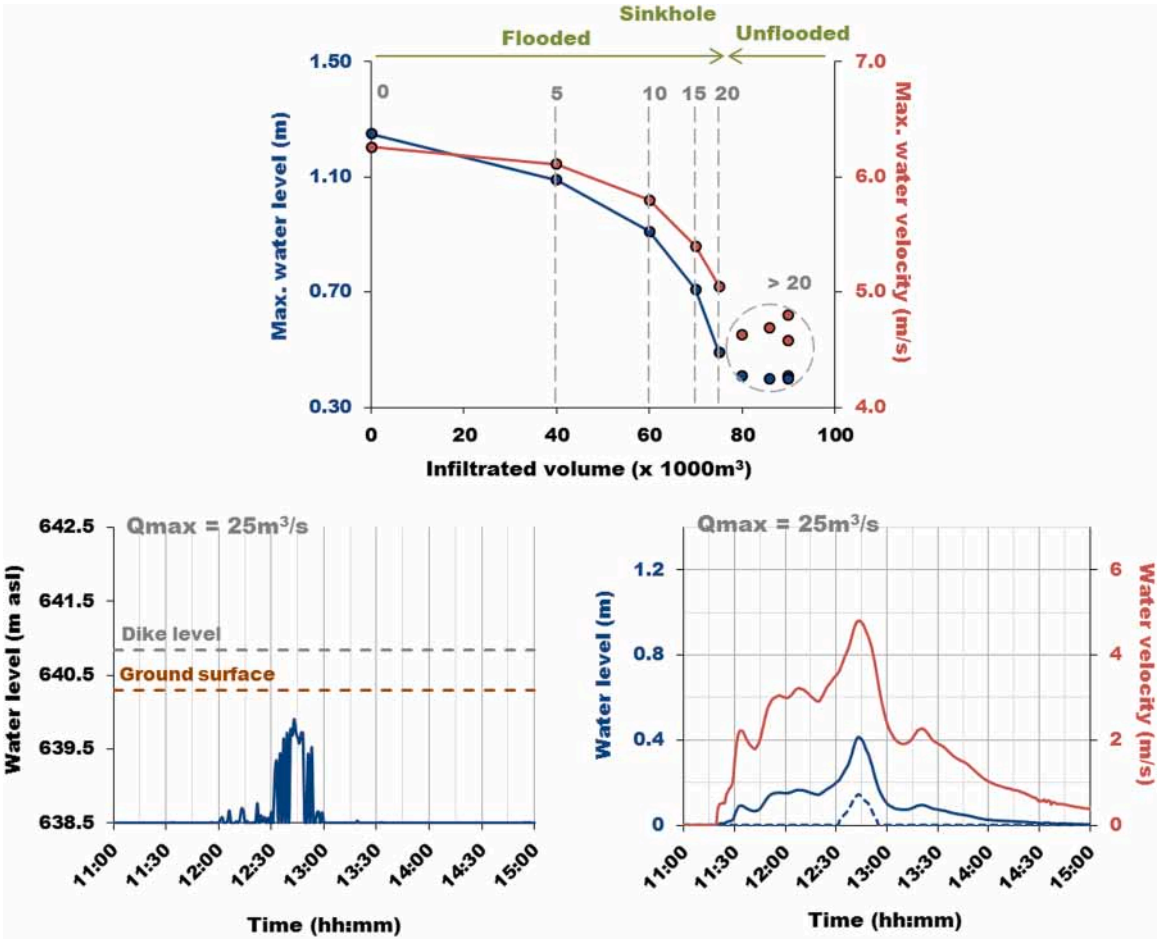

Fig. 7. Top graph: Maximal water levels (blue line) and velocities (red line) simulated in the main street for the Aug. 2015 event associated to different maximal drainage rates in the sinkhole (grey values in m^3/s). Over a rate of 20 m^3/s, the maximal conditions in the street remain approximately constant (due to runoffs from downstream of the dike). This can be related to the fact that for these rates the sinkhole remains unflooded (see water level in sinkhole for Qmax=25 m^3/s).

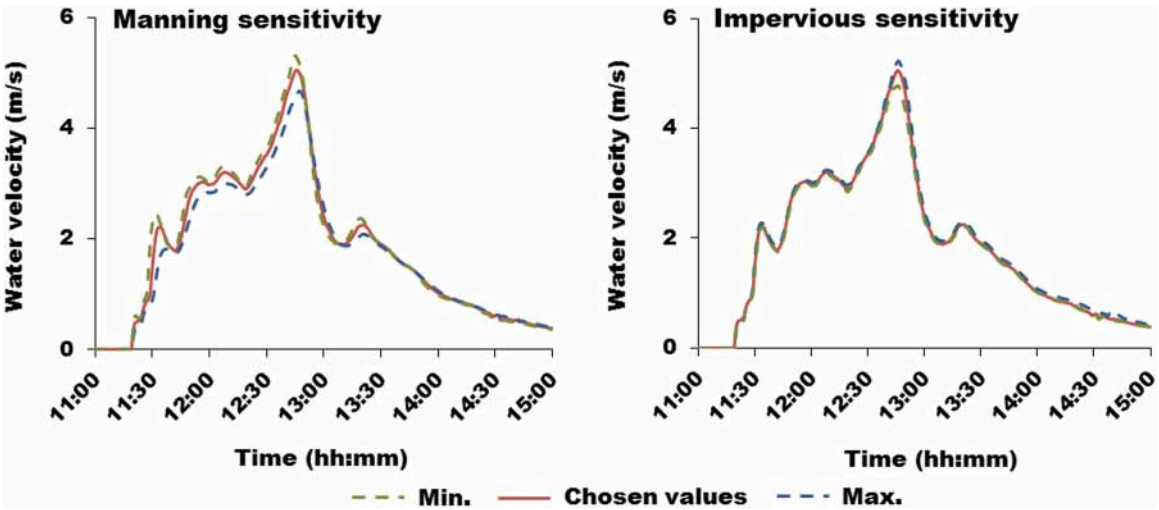

Fig. 8. Comparison between simulation results obtained with the chosen roughness and impermeability rate values and the minimal and maximal values of the ranges presented in Table 1. The results are mostly superimposed.

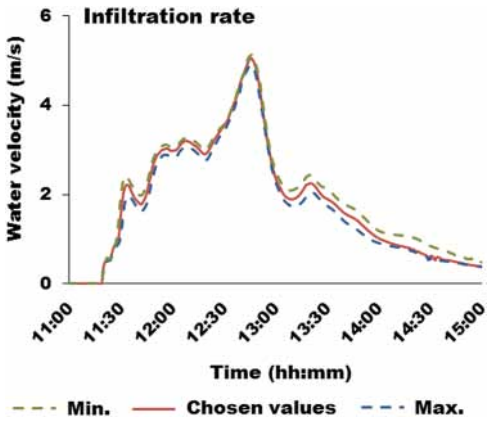

Fig. 9. Comparison between simulation results obtained with the chosen infiltration rate values and the minimal and maximal values of the ranges presented in Table 1. The results are mostly superimposed.

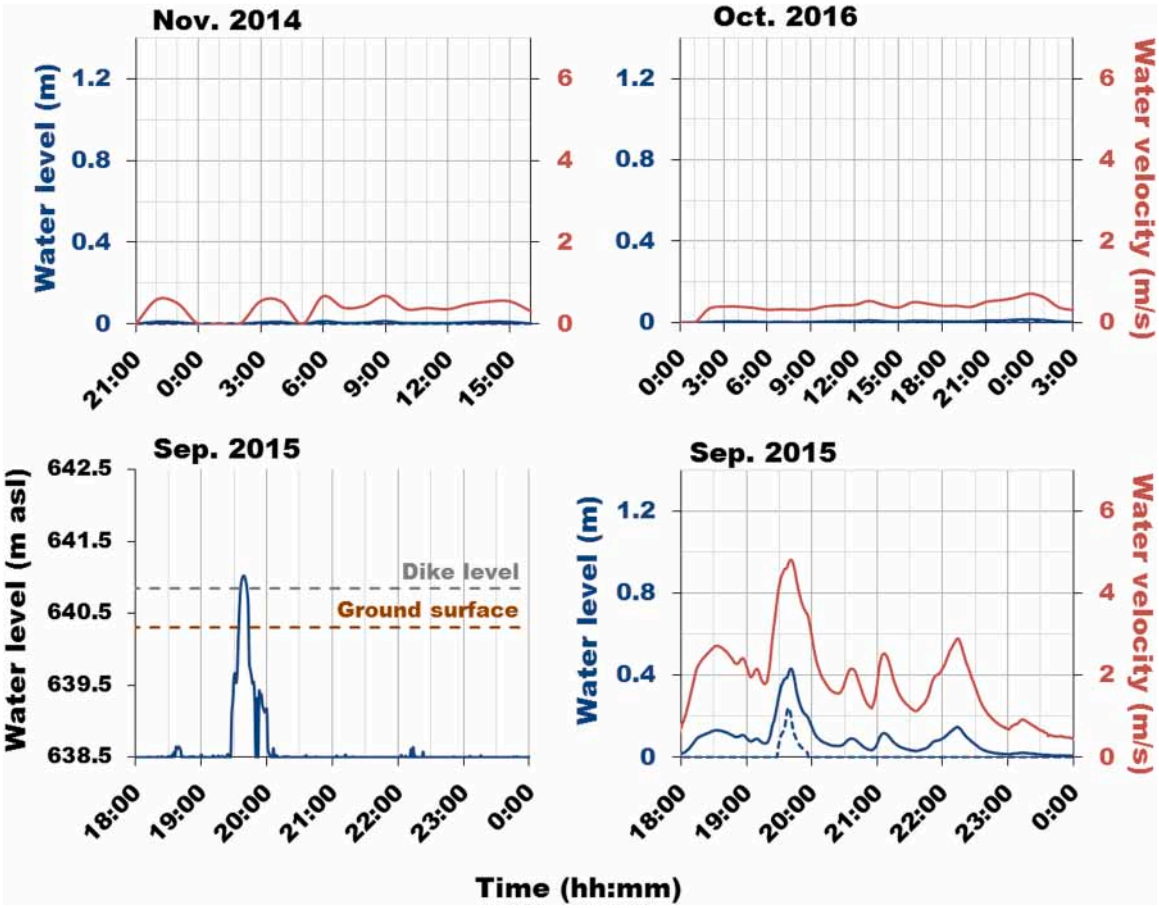

Fig. 10. Water level (in m) over time at the dike (dotted blue line) and in the street (full blue line) and velocity in the street (red line) simulated with the model for the Nov. 2014, Sep. 2015 and Oct. 2016 events. Bottom left: Water level (in m asl) over time in the South sinkhole during the Sep. 2015 event. The dike is submerged only during the Sep. 2015 event.

shows that, more than the total rain quantity, it is the intensity (thus quantity over duration) that determines if the village will be flooded or not. In particular the August 2015 and October 2016 events provided the same amount of water on the watershed, in the first case it resulted in a catastrophic flood, in the second case there was no runoff in the village.

In order to explain this difference of runoff behavior during different rainfall events, we used the simulation results in order to

Table 2
Comparison of the simulated maximal water levels at the dike and in the street and maximal velocities in the street for the different rainfall events.

Event	Duration (h)	Total rain (mm)	Mean intensity (mm/h)	Dike submersion (cm)	Max. water level village (cm)	Max. velocity village (m/s)
Nov. 14	20	142	7	0	1	0.7
Aug. 15	4	197	49	31	49	5.1
Sep. 15	8	276	35	24	43	4.8
Oct. 16	28	194	7	0	2	0.7

quantify the hydrological budget of the watershed for each event (Fig. 11). Note that, as the model does not take into account the underground fluxes (the underground storage and leakage capacities being considered as sufficiently high to not affect infiltration on the watershed), this budget only account for surface processes (runoffs and infiltrations).

When comparing the rainfall characteristics in Table 2 to the budgets in Fig. 10, it obviously appears that the rainfall intensity affects the becoming of water in the watershed. The higher the rain intensity, the higher the runoff, which is logical. However, it is interesting to see that in the cases of high intensities the proportion of water drained by the sinkhole becomes significantly higher and tends to limit this increase of runoff. Thus, even if the main intensity of the August 2015 event is 40% higher than the one of September, the runoff in the village remains in almost similar proportion for both events. As a result, this study case shows that, when it comes to quantify runoffs during extreme events, integrating the role of karst structures (here in particular the sinkhole) is crucial. On the contrary, the 2014 and 2016 low intensities events resulted in almost 90% of the water infiltrated in the soil over the watershed and thus, a relatively low impact of the karst structures.

4.4. Effect of rainfall intensity

We have taken advantages of the model in order to simulate different synthetic rain events, based on the Aug. 2015 hyetogram and conditions, in order to find the tipping rain intensity (i.e. starting to generate important runoff in the village when the dike is submerged) in this specific study case. Therefore, we have first tested different rainfall scenarii described in Table 3. These scenarii are applied based on the exact same assumptions than for the Aug. 2015 event that infiltrated and absorbed water are never limited by underground storage capacities. Thus, the total rain amount considered for these synthetic rain events remain in a same order or less than the true historical event.

The synthetic cases show that the maximal rain intensity before dike submersion in this study case is 110 mm/h. In fact, when performing simulations with 1 h uniform rains at this intensity or below, the dike remains unflooded, even when increasing the rainfall duration. However, when considering a 120 mm/h rainfall, the dike is submerged. This is further validated by the fact that when one simulates the August 2015 event but clipping all intensities above 110 mm/h (12% of the event), the dike also remains unflooded.

It is also interesting to show the effect of rainfall sub-hourly variability. In fact, when testing a triangular rain shape for a 1 h rainfall (rain intensity increases from 60 to 140 mm/h before decreasing back to the initial value within 1 h), the dike is also submerged even if the total quantify of rain over the event is the same as a 100 mm/h uniform event that would not generate this submersion. This shows that, for extreme event with high variabilities over short amount of time, it is necessary to measure precisely these variations. As an illustration of this fact, when simulating the August 2015 event with an hourly averaged rainfall, the results indicate that the village would not be significantly flooded.

5. Discussion

This study case presents several advantages for the setup of a spatial model of surface runoffs and their relation to the underground systems. The watershed is relatively small (1 km^2), it can be easily explored to identify the different biomes and karst features. It also allows to constrain the model properties with several spatially distributed field measurements. The small village, mainly built along one main street, is located at the outlet of the watershed. Furthermore, the houses on either sides of the main street are built one against the other. Thus, the main street of the village forms a giant Venturi channel that collect all runoffs during the flood events where they can be quantified. Finally, flash flood events can rarely be measured because of their very limited time scale (hourly scale). Nevertheless, the Aug. 2015 flash flood in this watershed has been widely documented in time and space (based on ocular observations but also several videos providing the water velocities). This documentation could be used as a basis for the model calibration. However, the uncertainties of the model can barely be quantified because of the limited amount of data for such flash floods events, the rainfall events responsible for such floods having a return period of more than 100 years. Thus, the model could be validated with three other rain events only qualitatively (submersion of the dike or not). Nevertheless, the sensitivity analysis performed on the input parameters of the model (infiltration rates, roughness, impervious surfaces) showed that the simulation results were rather insensitive to variations of these inputs, thus suggesting that the modelling of runoffs for such events is mostly conditioned to the topography of the watershed and the absorptions in the sinkholes. The first parameter is well known in this study case, as we could use a high resolution digital terrain model of the area. The second parameter was then calibrated on the Aug. 15 event observations. As a result, if the produced model could barely be validated, it remains sufficiently constrained to be representative.

In order to perform the simulations, some simplifications of the model, presented in Section 3.1, have been adopted. In small watersheds like in this case, considering a uniform rainfall is acceptable. Likewise, neglecting the evapotranspiration during rainfall events will not generate important errors in the results. The assumption of constant diffuse infiltration in soils adopted for this model

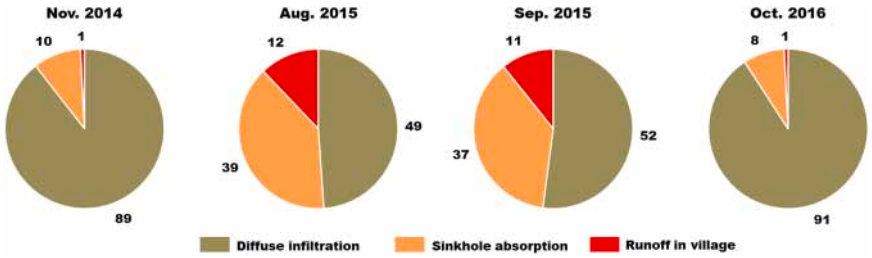

Fig. 11. Simulated water balances (diffuse infiltration in soils, punctual infiltration in sinkhole or runoff) for the different rainfall events. Values are in %.

Table 3
Comparison of the simulated maximal water levels at the dike and in the street and maximal velocities in the street for different simple synthetic cases and for the Aug. 2015 event considering some modifications in the hyetogram: truncation of intensities over 110 mm/h or considering a hourly time step hyetogram instead of a 6 min time step.

Rainfall (mm/h)	Duration (h)	Total rain (mm)	Dike submersion (cm)	Max. water level village (cm)	Max. velocity village (m/s)
SYNTHETIC CASES					
100	1	100	0	17	3.2
100	2	200	0	17	3.2
110	1	110	0	19	3.4
120	1	120	3	21	3.6
Triangular (60–140)	1	100	5	23	3.7
AUG. 15 EVENT					
Aug. 2015	4	197	33	49	5.1
Aug. 2015 (<110 mm/h)	4	170	0	19	3.4
Aug. 2015 (1 h)	4	197	3	21	3.7

could also be a source of simulations uncertainties. If considering the soil to become quickly saturated during a rainfall remains acceptable, in such watershed with important slopes it is possible that a small part of the infiltrated water is restituted in the talweg within a same rainfall event (as interflows or hypodermic runoffs). It is however complex to quantify without spatial measurements of water levels along the stream paths and it may represent only a very limited part of the total water volume.

However, this study case presented a particular configuration that allowed considering important simplifications that can usually not be generalized. In particular the watershed is at a relatively high altitude and, thus, its karst features are dry over 500 m high. Furthermore, the considered rainfall events in this study (and especially the most intense ones) happened at the end of summer, thus when the underground are the driest and the saturated water table in the karst network is very low. These particularities allowed considering that the saturated water table was low enough to not affect drainage in the sinkholes of the watershed during these rainfalls. At lower altitudes, or at wetter periods of the year, this assumption could generate important errors in the simulations and groundwater level should be taken into account. It could reduce the drainage rate over time, or even inverse the surface-underground exchanges (sinkhole becoming a karst network discharge at the surface) in some cases (Jourde et al., 2007; Maréchal et al., 2008; Bailly-Comte et al., 2009).

6. Summary and conclusion

This work presents a hydrological study case of runoffs quantification for different rainfall conditions in a small mountainous karstic watershed. This quantification relies on a spatial physical-based numerical model. This small basin dimension makes it possible to accurately assess the different hydrodynamic factors spatially conditioning water fluxes and exchanges (topography, soil conductivity, roughness). The most important remaining unknown is the drainage capacity of the karst sinkholes located near the outlet the basin. However, runoffs descriptions and observations in the village, located at the outlet of the basin, during four different rainfall event (and especially during one catastrophic event in 2015) allows to calibrate the punctual infiltration rate associated to the sinkholes in the model.

The model has then be used to quantify the water balances (diffuse infiltration, sinkhole drainage or runoffs) for this study case during four rain events characterized by different intensities but similar total cumulated rainfalls. The simulations show that for the two long and low intensity rain events a majority of water (approx. 90%) infiltrates the soil as diffuse infiltration, a lower part is drained into the karst network (approx. 10%) and a negligible part (< 1%) runoffs. However, for the two short and intense rain events, the water balance drastically changes as the diffuse infiltration part is decreased (approx. 50% instead of 90%) in favor of runoff (reaching approx. 10%). In such events the direct drainage into the karst plays a significant role as it reduces surface runoff by absorbing a larger part of total water (approx. 40% instead of 10%). An analysis with synthetic rain events shows that it is not the total amount of fallen water that affects the generation of floods in the village but rather the exceeding of a critical rainfall intensity during the event. In the same idea, we show that using hyetograms at hourly time steps for such short and intense events generates totally

inaccurate and underestimated simulations as it tends to average intensity variability within an hour.

This study is not totally generalizable as our study site allowed several numerical simplifications, in particular that infiltration rate through sinkholes remained constant during rains events (while in general this rate is affected by the groundwater table level and can be in the opposite way under particular conditions). Thus, a similar approach could be applied in similar watershed configurations, mainly in karstified calcareous Plateau or mountainous areas, with important thickness of unsaturated conduits network separating the entries (sinkholes) and the exit (spring).

However, this study shows with an application how the hydrological water balance can be significantly affected by the intensity variations during a rain event in a karst watershed. Furthermore, as other references on this topic, it also shows that taking into account the local fast exchanges between surface and underground through karst connections becomes crucial during extreme events.

CRediT authorship contribution statement

Pierre Fischer: Conceptualization, Methodology, Validation, Visualization, Writing – original draft. **Séverin Pistre**: Conceptualization, Validation, Writing – review & editing, Funding acquisition. **Pierre Marchand**: Resources, Writing – review & editing.

Declaration of Competing Interest

The authors declare that they have no known competing financial interests or personal relationships that could have appeared to influence the work reported in this paper.

Data Availability

Data will be made available on request.

Acknowledgments

This work would not have been possible without the dedication of Dr. Marc Leblanc and we thank him for his help. We would like to thank the students who have participated to this study through different projects and internships: Timéo, Blandine, Thibault, Virginie and Rémi. We thank two anonymous reviewers and the editor for their valuable suggestions during the review process.

Appendix A. Supporting information

Supplementary data associated with this article can be found in the online version at doi:10.1016/j.ejrh.2022.101206.

References

Al Aamery, N., Adams, E., Fox, J., Husic, A., Zhu, J., Gerlitz, M., Agouridis, C., Bettel, L., 2021. Numerical model development for investigating hydrologic pathways in shallow fluviokarst. J. Hydrol. 593, 125844.

Bailly-Comte, V., Jourde, H., Pistre, S., 2009. Conceptualization and classification of groundwater–surface water hydrodynamic interactions in karst watersheds: Case of the karst watershed of the Coulazou River (Southern France). J. Hydrol. 376, 456–462.

Bailly-Comte, V., Borrell-Estupina, V., Jourde, H., Pistre, S., 2012. A conceptual semidistributed model of the Coulazou River as a tool for assessing surface water–karst groundwater interactions during flood in Mediterranean ephemeral rivers. Water Resour. Res. 48, W09534 https://doi.org/10.1029/2010WR010072.

Bois, P., Obled, C., De Saintignon, M.F., Mailloux, H., 1997. Atlas expérimental des risques de pluie intenses: Cévennes-Vivarais. LTHE-LAMA, pôle grenoblois d'étude et de recherche pour la prévention des risques naturels. EDF-DTG 19.

Camus, H., 1997. Formation des réseaux karstiques et creusement des vallées: L'exemple du Larzac méridional, Hérault, France. Karstologia 29, 23–42.

Field, M.S., 2010. Simulating drainage from a flooded sinkhole. Acta Carsol. 39, 361–378.

Fleury, P., Maréchal, J.C., Ladouche, B., 2013. Karst flash-flood forecasting in the city of Nîmes (southern France). Eng. Geol. 164, 26–35.

Ford, D.C., Williams, P., 2007. Karst Hydrogeology and Geomorphology. John Wiley, Chichester, p. 562. https://doi.org/10.1002/9781118684986.

Gutiérrez, F., Parise, M., De Waele, J., Jourde, H., 2014. A review on natural and human-induced geohazards and impacts in karst. Earth-Sci. Rev. 138, 61–88.

Hazen, A., Williams, G.S., 1920. Hydraulic Tables. John Wiley and Sons, New York.

Jourde, H., Roesch, A., Guinot, V., Bailly-Comte, V., 2007. Dynamics and contribution of karst groundwater to surface flow during Mediterranean flood. Environ. Geol. 51, 725–730.

Klimchouk, A.B., 1995. Karst morphogenesis in the epikarstic zone. Cave and Karst. Cave Karst Sci. 21, 45–50.

Lassabatère, L., Angulo-Jaramillo, R., Soria Ugalde, J.M., Cuenca, R., Braud, I., Haverkamp, R., 2006. Beerkan estimation of soil transfer parameters through infiltration experiments – BEST. Soil Sci. Soc. Am. J. 70, 521–532.

Le Coz, J., Hauet, A., Pierrefeu, G., Dramais, G., Camenen, B., 2010. Performance of image-based velocimetry (LSPIV) applied to flash-flood discharge measurements in Mediterranean rivers. J. Hydrol. 394, 42–52.

Le Coz, J., Jodeau, M., Hauet, A., Marchand, B., Le Boursicaud, R., 2014. Image-based velocity and discharge measurements in field and laboratory river engineering studies using the free FUDAA-LSPIV software. River Flow. 7 (Lausanne, Switzerland).

Leblanc, M., 2018. Histoires d'eau à la Vacquerie et St Martin de Castries. CPIE Causses Méridionaux, Collect. Mémoire De. Territ. 148 (pages. Occitanie Region, France).

Li, X.-Y., Contreras, S., Solé-Benet, A., Canton, Y., Domingo, F., Lazaro, R., Lin, H., Van Wesemael, B., Puigdefabregas, J., 2011. Controls of infiltration–runoff processes in Mediterranean karst rangelands in SE Spain. Catena 86, 98–109.

Liu, Y.B., Batelaan, O., De Smedt, F., Huong, N.T., Tam, V.T., 2005. Test of a distributed modelling approach to predict flood flows in the karst Suoimuoi catchment in Vietnam. Environ. Geol. 48, 931–940.

Malcles, O., Vernant, P., Chéry, J., Ritz, J.-F., Cazes, G., Fink, D., 2020. Burial ages, ghost-rocks and karst network structure. Insights from the Vis canyon (Southern France). Géomorphologie: Relief Process. Environ. 26, 255–264.

Maréchal, J.C., Ladouche, B., Dörfliger, N., 2008. Karst flash flooding in a Mediterranean karst, the example of Fontaine de Nîmes. Eng. Geol. 99, 138–146.

Palanisamy, B., Workman, S.R., 2015. Hydrologic modeling of flow through sinkholes located in streambeds of cane run stream, Kentucky. J. Hydrol. Eng. 20, 04014066 https://doi.org/10.1061/(asce)he.1943-5584.0001060.

Wang, S., Fu, Z., Chen, H., Nie, Y., Xu, Q., 2020. Mechanisms of surface and subsurface runoff generation in subtropical soil-epikarst systems: Implications of rainfall simulation experiments on karst slope. Journal of Hydrology 580, 124370. https://doi.org/10.1016/j.jhydrol.2019.124370.

White, W.B., 2002. Karst hydrology: recent developments and open questions. Eng. Geol. 65, 85–105.

Zhou, W., 2007. Drainage and flooding in karst terranes. Environ. Geol. 51, 963–973.